journal of the international meteor organization

WGN

47:3
june 2019

Meteorite-dropping fireball over Poland on 2018 Oct 5/6
Perseid fireball of 2018 Aug 13 seen by video, photo, and radar
May-June IMO video meteors
Meteor reports in The Astronomer magazine - part IV

ISSN 1016-3115

WGN Vol. 47, No. 3, June 2019, pp. 75 – 106

Fireballs

PF061018 Bukienka – meteorite dropping fireball *A. Olech, P. Żołądek, M. Wiśniewski, H. Krygiel, M. Kwinta, M. Myszkiewicz, P. Nowak, K. Polak, K. Polakowski, A. Raj, M. Szlagor, J. Twardowski, and Z. Tymiński* 75

3414-2018: A Perseid fireball showing exceptional light effects, observed by video, photo and radio *Peter C. Slansky and Bernd Gaehrken* 79

Preliminary results

Results of the IMO Video Meteor Network — May 2018 *Sirko Molau, Stefano Crivello, Rui Goncalves, Carlos Saraiva, Enrico Stomeo, Jörg Strunk, Javor Kac* 93

Results of the IMO Video Meteor Network — June 2018 *Sirko Molau, Stefano Crivello, Rui Goncalves, Carlos Saraiva, Enrico Stomeo, Jörg Strunk, Javor Kac* 98

History

A History of Meteor Reports in The Astronomer magazine: part 4: 2000–2012 *Tracie Heywood* 102

Front cover photo

Brilliant fireball captured on 2019 February 26 at $06^{h}14^{m}$ UT, from Vilaflor, Santa Cruz de Tenerife, Canary Islands. Photo courtesy: Hermann Koberger.

Writing for WGN

This Journal welcomes papers submitted for publication. All papers are reviewed for scientific content, and edited for English and style. Instructions for authors can be found in WGN **45:1**, 1–5, and at `http://www.imo.net/docs/writingforwgn.pdf` .

Copyright

Legal address

International Meteor Organization, Jozef Mattheessensstraat 60, 2540 Hove, Belgium.

3414-2018: A Perseid fireball showing exceptional light effects, observed by video, photo and radio

Peter C. Slansky[1] *and Bernd Gaehrken*[2]

This article is about the observation of 3414-2018, a 2018 Perseid fireball, with video, photo and radio in parallel from three different observing sites so that the trajectory could be calculated. The fireball showed exceptional light effects, including a very bright terminal flash with a radius of up to 4 km, a persistent train, a green afterglow and a diffuse, widespread bluish sky glow with a radius of more than 120 km, persisting for up to half a second. These observations were possible only by the use of two very high sensitive cameras in video mode with full HD resolution in colour independently.

Received 2019 February 9

1 Introduction

Fireball patrol has become popular. Some fireball events have been reported by more than a thousand people. So far, the all-time No. 1 on the IMO fireball website is event 4299-2017 (IMO, 2017) over Frankfurt, Germany, reported by 2046 observers from eight European countries, followed by event 3638-2014 (IMO, 2014) over Pittsfield, Massachusetts, USA, reported by 1547 observers from the US and Canada. Other fireballs gain celebrity status when new observation techniques facilitate new information about their physical nature. Hence, a 2001 Leonid became famous because it was observed with an intensified high speed video camera at 1000 frames per second, revealing an axe-shaped shock halo of a meteor head for the first time (Jenniskens & Stenbaek-Nielsen, 2004). EN120812, a −9 mag 2012 Perseid fireball, became the "haul" of no less than 17 professional meteor cameras in Czechia (Spurný et al., 2014), revealing a record breaking entering altitude of 170 km and a lot of other detailed information. Both observations induced a lot of scientific papers including new models of the physical principles of meteor light distribution. Also in this article, there will be further references to these events.

The main character of this article is a Perseid fireball that lighted up on 2018 August 13 at 01^h51^m UT over Ingolstadt, Southern Germany (IMO, 2018). To the knowledge of the authors only two visual observations were reported (not by the authors, unfortunately). But it was recorded by amateurs (alone) with three different observation techniques, independently: Photography, video and radio – still a quite rare parallelism. After the report to the IMO by the authors this fireball gained IMO code 3414-2018. By a joint examination together with two other German amateurs, Juergen Michelberger and Reinhardt Wurzel, who had observed it as well, 3414-2018 turned out to be an outstanding specimen of the rich family of the Perseids: It entered the atmosphere at a height of 159 km, produced a terminal flash of −7 mag (according to Wurzel (2019)) at a height of 82 km and expired at a height of 77 km, leaving behind a persistent train that was visible for about 3 minutes and more than 7 minutes on a photo series. The terminal flash was accompanied (respectively followed) by a strong green afterglow with a comparably sharp outline with a radius of up to 4 km. Even more astonishing, the terminal flash and the green afterglow were not just reflected by the atmosphere but were accompanied (respectively followed) by a widespread bluish sky glow that persisted up to 480 ms, recorded by two cameras independently, up to a distance of 122 km from the point of the terminal flash. The areal dimensions of the light distribution of 3414-2018 were so exceptional that the authors made a line of technical tests to rule out camera or lens artefacts, what the tests definitively did. The meteor was also observed by a radio amateur from Dessau, Middle Germany, who had his antenna pointed to the GRAVES radar in France. The train echo lasted 43 s and showed a significant Doppler shift. So, further examination of 3414-2018 seems to be highly valuable.

2 Observation

The first report of this fireball to the IMO came from the authors. We had observed the 2018 Perseids in the first night on August 11/12 from Oberes Sudelfeld, Bavarian Alpine Mountains, 1420 m altitude. Due to the weather forecast for the second night on August 12/13, we moved to Geigersau, Upper Bavaria, 930 m altitude (47.72701° N / 11.02595° E). At 03^h51^m CEST (= 01^h51^m UT) we were both busy with a technical camera test. So, we missed the sight of our brightest 2018 Perseid. We only saw the reflection of its terminal flash on the ground like a flash light. Luckily, it turned out that this fireball had been covered by the fields of the two high sensitivity digital cameras Sony α7S running in video mode (Figure 1) and also, for the most part, by a photo camera Canon EOS M (Figure 3). The video of 3414-2018 was presented by Peter C. Slansky on the IMC 2018 in Pezinok, Slovakia (Slansky, 2019).

The Sonys had recorded more than 500 meteors in the two Perseids nights, but when the videos were analyzed, the fireball at 01^h51^m UT caught our special attention because of its exceptional light effects (Figure 2). Although both authors had missed the fireball visually, we reported it to the IMO and uploaded our videos and photos. By this "our" fireball became 3414-2018 – ready to be shared with the meteor observers' community.

Soon we were happy to hear from Juergen Michelberger and Reinhardt Wurzel who had observed 3414-

[1]Email: slansky@mnet-online.de
[2]Email: bgaehrken@web.de

IMO bibcode WGN-473-slansky-fireball
NASA-ADS bibcode 2019JIMO...47...79S

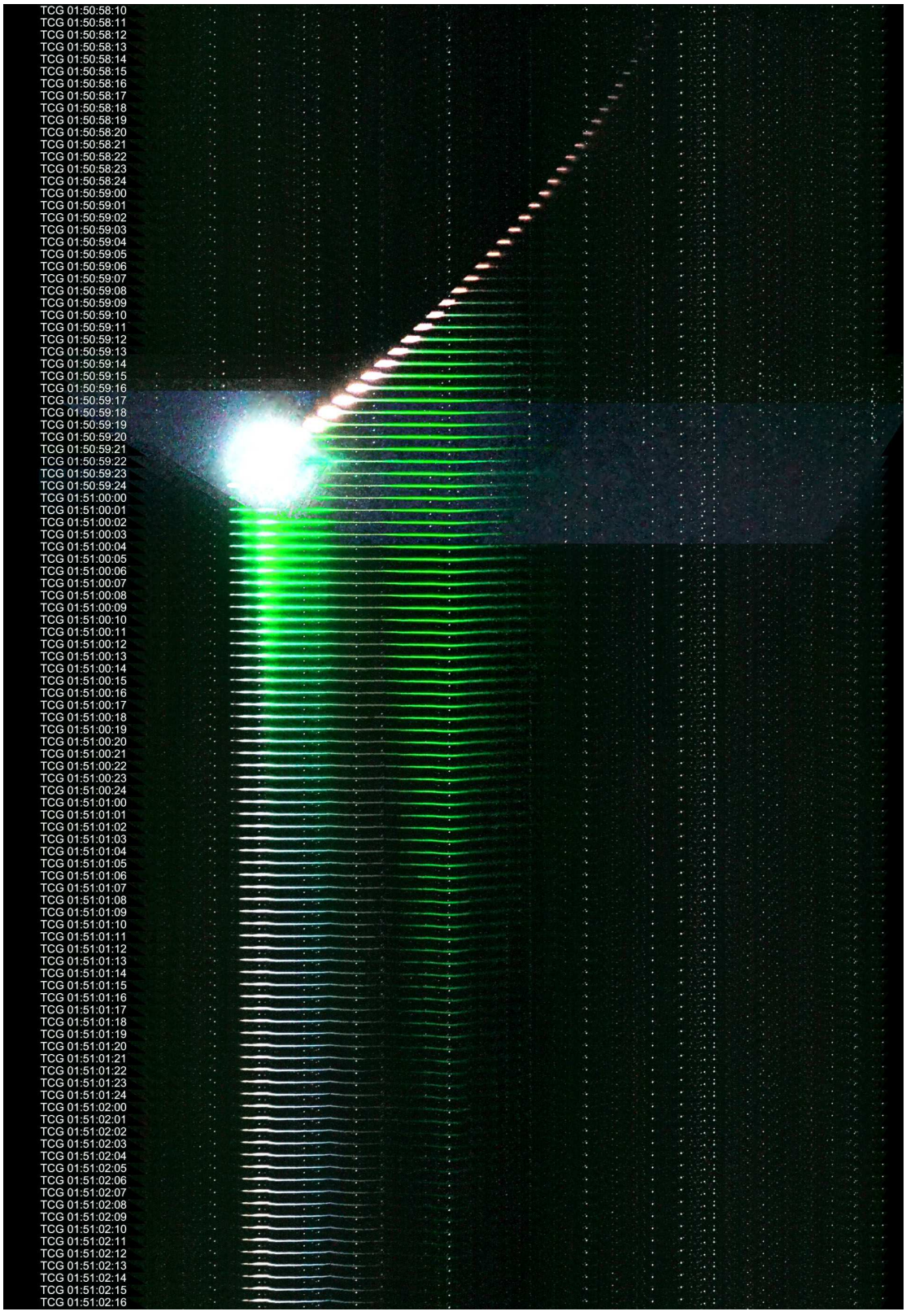

Figure 1 – Sequence analysis of fireball 3414-2018 on 2018 August 13, $01^{h}51^{m}$ UT, observed by Peter C. Slansky at Geigersau, Upper Bavaria, Germany, together with Bernd Gaehrken. The original video was shot with two Sony α7S cameras at 25 fps with $t = 1/25$ s and ISO 409 000, equipped with two Canon FD 1.4/50mm lenses at $F = 1.4$. The meteor appeared in the field of view of camera 1, pointing to Camelopardalis in the image center, from right to left. Then it changed to the field of view of camera 2, pointing to Ursa Minor, where it ended in a terminal flash. The embedded real time code (UT) indicates the temporal development in hours:minutes:seconds:frames. The time of a radio clock had been transferred manually to the time code setting of the cameras with an estimated precision of about 250 ms. The images were rotated clockwise so that the meteor proceeds exactly from right to left in the composite. Hence, in this composite every vertical step from top to bottom represents a temporal step of 1/25 s = 40 ms. In every image a line of stars appears. To show the dimensions of the – strongly overexposed – terminal flash five frames around frame 01:50:59:22 are shown as an overlay on the rest of the sequence analysis (note the additional stars appearing only in these five wider stripes).

Figure 2 – The terminal flash of 3414-2018 in a compositing of two single video frames of camera 1 (right) and camera 2 (left). The image center of camera 1 pointed to Camelopardalis, the image center of camera 2 to Ursa Minor. The border between the two camera fields is visible on the beginning of the green train. The bright star slightly right from the image center is Polaris. It has "wings" due to artefacts of the lens (curvature of field, astigmatism and coma). On the right and upper side of the white clipped area of the terminal flash block-shaped data compression artefacts can be seen. They are caused by the recording codec of the camera. The widespread bluish sky glow that appears in the fields of view of both cameras is no artefact. It will be examined in detail in Section 4.6.

Figure 3 – Persistent train of 3414-2018 photographed by Bernd Gaehrken in a series from Geigersau with a Canon EOS M at ISO 3200 with 15 s integration time with Canon 2.8/50mm lens set to $F = 2.8$ (Gaehrken, 2018). The persistent train was warped by wind. Please also note the changes in colour. It will be described in detail in Section 4.7.

2018 visually and had photographed it, too (Figure 4). Their observing site had been Horní Vltavice, Czechia, at 822 m altitude (48.952° N /13.765° E). By a lucky coincidence, our observing directions were rectangular: we, "team Geigersau", had pointed our cameras to the North, catching the fireball in Ursa Minor, "team Horní Vltavice" had pointed their camera (and their eyes) to the West with the fireball appearing in Sagitta/Aquila. With the video from Geigersau and the photo from Horní Vltavice, Juergen Michelberger calculated the trajectory. Reinhardt Wurzel provided additional information about the atmosphere, while the authors started a qualitative and quantitative analysis of the videos and photos.

Team Geigersau operated two Sony α7S equipped with Canon FD 1.4/50 mm lenses set to $F = 1.4$. According to earlier experiences (Slansky, 2016), the cameras were run with 25 frames per second with an exposure time of 1/25 s at the maximum sensitivity ISO 409 000. In earlier tests this camera-lens combination – with the lens stopped down to $F = 2.0$ – had achieved a stellar limiting magnitude of 8.7 mag (Slan-

Figure 4 – 3414-2018 photographed by Juergen Michelberger from Horní Vltavice, Czechia, together with Reinhardt Wurzel, with a Canon EOS 700D at ISO 1600 and 60 s exposure time with a Tamron 2.8/17-50mm zoom lens at $f = 17$ mm and $F = 2.8$. The exact exposure interval was from $01^h50^m32^s$ to $01^h51^m32^s$ UT ± 1 s. The camera was pointing to the West, so the fireball appears in the constellations Sagitta/Aquila. Unfortunately, there was some dew on the front lens.

sky, 2018a). Both cameras were mounted on a parallactic mounting with the long axis of the fields orientated towards the radiant in an angle so that Polaris was in the overlap of both camera fields on the short axis. A focal length of 50 mm provided a field of view of 39.0° × 22.7° at an aspect ratio 16:9 on the Sony's sensors. With this camera-lens combination the angular resolution was 1.24 arcminutes per pixel, corresponding to 48.45 pixels per degree.[a] The recording was done in full HD resolution 1920 × 1080 pixels via internal recording with XAVC S, 50 Mbit/s, 8 bit per channel.

Additionally, a Canon EOS M photo camera was mounted on another parallactic mounting. It was equipped with a Canon 2.8/50mm lens at $F = 2.8$. This camera was operated in a series with an exposure time of 15 s at ISO 3200. The fireball flew through the camera's field of view with the terminal flash outside but the biggest part of the persistent train was captured for seven minutes until the photo series was interrupted by technical reasons.

[a]This is an average value; according to the laws of perspective the angular resolution varies from the center of the image to the periphery.

Team Horní Vltavice used a Canon EOS 700D on a parallactic mounting with a Tamron zoom lens 2.8/17-50mm set to $f = 17$ mm and $F = 2.8$. The field of view was 47.3° × 66.5° at a resolution of 3456 × 5184 pixels. The camera was set to ISO 1600 with 60 s exposure time in a series. The exact exposure interval was from $01^h50^m32^s$ to $01^h51^m32^s$ UT ± 1 s. Unfortunately, there was some dew on the front lens. But the image was still usable. By a lucky coincidence, the cameras of team Geigersau and team Horní Vltavice were crossing their optical axis' at an angle of nearly 90° and the meteor crossed them at an angle of nearly 45° resulting in ideal geometrical conditions for the calculation of the trajectory.

3 Trajectory

Due to the differences in exposure the meteor head became visible in the video from Geigersau much earlier than in the photo from Horní Vltavice, as can be seen in Figure 6. According to this, Juergen Michelberger calculated the trajectory along four points:

- Point A: Meteor becomes visible in the video of Peter C. Slansky with a Sony α7S from Geigersau
- Point B: Meteor becomes visible in the photo of Juergen Michelberger with a Canon 700D from Horní Vltavice
- Point C: Terminal flash
- Point D: Expiration of the meteor.

Point D could be detected clearly in the photo as well as in the video. Due to the movement of the meteor, Point C had to be calculated from the centroid of the overexposed area of the terminal flash in both the photo and the respective frame of the video.

The meteor flight between point A and D was recorded over 39 video frames = 1560 ms. But the starting point A had to be interpolated between two video frames. So, the real duration of the meteor flight was

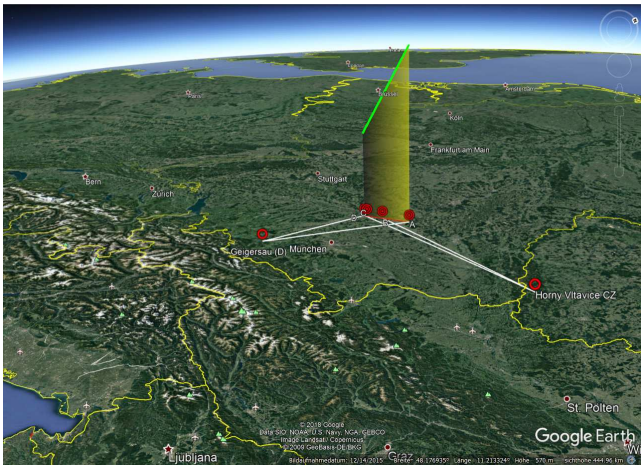

Figure 5 – Trajectory of 3414-2018 (green) with points A, B, C and D projected to the ground (red) and the projected viewing angles (white) from the two observation sites (red circles).

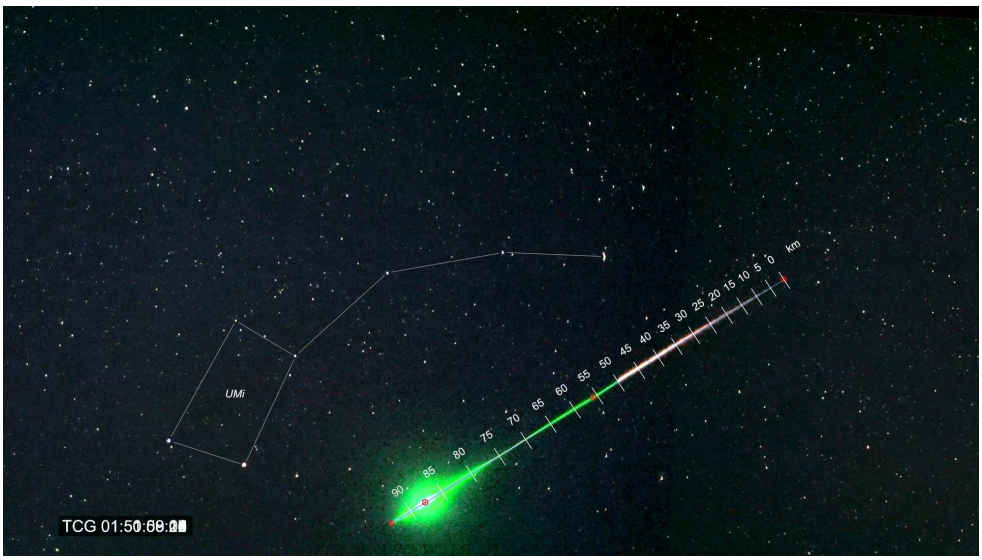

Figure 6 – Trajectory of 3414-2018 in the video from Geigersau with points A, B, C and D (red) and with the real length in km starting from point A (= 0 km). The entry point A indicates where the meteor became visible. It lies inside the integration time of 40 ms of video frame 01:50:58:11 UT [hh:mm:ss:ff].

38.3 frames = 1532 ms. In this time the meteor traveled a distance of 92.9 km. This means an average geocentric speed v_m = 60.6 km/s. It has to be taken into account, that the duration of half a video frame (= 20 ms) causes a difference in speed of 0.8 km/s. Closer examination revealed a speed between point A and B v_{AB} = 61.9 km/s and a speed between point B and D v_{BD} = 58.9 km/s. An amount of 0.11 km/s goes back to earth rotation. Hence, 3414-2018 was slightly faster than the literature speed values for Perseids ranging from 59 km/s (Rendtel, 2017) to 60 km/s (Hughes, 1995). The speed distribution of 3414-2018 between entry, terminal flash and expiration matches well with the 2012 Perseid fireball observed by Spurný et al. (2014).

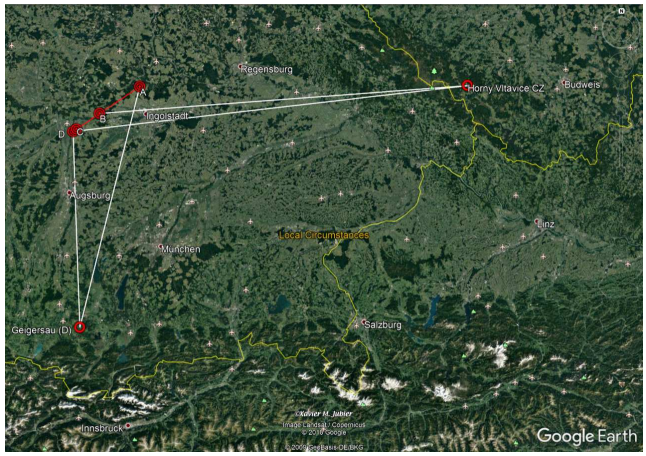

Figure 7 – Trajectory of 3414-2018 projected onto the ground (red). Note, that the fireball was recorded by the video camera from Geigersau via the angle A-D but by the photo camera from Horní Vltavice via the sharper angle B-D (both white).

4 Light distribution

4.1 Meteor head

According to Figure 1 the meteor head becomes visible in the video at frame 01:50:58:12 at an altitude of 158.6 km. The average motion blur of the meteor in each video frame is about 21 pixels. Due to the laws of perspective, the angular velocity of the meteor head in the video increases slightly when the meteor flies from the image corner to the image center. In the following 19 frames (= 760 ms), down to an altitude of 116.9 km, neither a wake nor a train occurs.

Between frames 01:50:59:07 and 01:50:59:16 (for 360 ms) the meteor shows a trapezoid shape. This is quite remarkable, because this artefact – just like the "wings" of Polaris in Figure 2 – is caused alone by lens defects such as curvature of field, astigmatism and coma. The occurrence of this artefact states, firstly, that the meteor is becoming significantly overexposed at the beginning of the occurrence of the artefact and secondly, that the meteor head still appears as a point shaped object until the artefact ends. According to the camera and lens tests that were made by the authors, blooming caused by the camera sensor or the lens have to be excluded as a reason. So, after the vanishing of this artefact, from frame 01:50:59:16 on at an altitude of 94.9 km, the meteor head has to be seen as an areal object that is spatially resolved by the camera. Due the clipping caused by overexposure the exact shape of the meteor head cannot be determined from the video image, but significant hints are revealed in the following.

4.2 Wake

To differentiate the meteor head, the white wake and the green train it is evident that a colour video camera provides significant advantages. Due to the motion blur, the wake is not resolved sharply. A very short white wake can be seen at first in frame 01:50:59:05 at an altitude of 119.1 km. "White" is referred to the white balance of the camera which was daylight of approximately 6000 K. In the beginning the wake's length is shorter than the motion blur. So, its duration is less than 40 ms. In the following frames the wake becomes a little longer but is followed by the green train so quickly that they cannot be separated precisely.

Table 1 – Trajectory and additional parameters of 3414-2018.

Time code (UT) [hh:mm:ss:ff]	Distance from meteor entry at the start of frame [km]	Height [km]	Comments
01:50:58:11	−1.8	160.2	Point A
01:50:58:12	0.7	158.0	
01:50:58:13	3.1	155.8	
01:50:58:14	5.5	153.7	
01:50:58:15	8.0	151.5	
01:50:58:16	10.6	149.2	
01:50:58:17	13.2	147.0	
01:50:58:18	15.7	144.8	
01:50:58:19	18.1	142.7	
01:50:58:20	20.5	140.6	
01:50:58:21	22.9	138.4	
01:50:58:22	25.3	136.3	
01:50:58:23	27.7	134.2	
01:50:58:24	30.0	132.2	
01:50:59:00	32.5	130.0	
01:50:59:01	34.9	127.9	
01:50:59:02	37.3	125.8	
01:50:59:03	39.8	123.5	
01:50:59:04	42.3	121.4	
01:50:59:05	44.9	119.1	
01:50:59:06	47.4	116.9	
01:50:59:07	49.8	114.8	
01:50:59:08	52.3	112.6	
01:50:59:09	54.9	110.3	Point B
01:50:59:10	57.6	108.0	
01:50:59:11	60.2	105.7	
01:50:59:12	62.7	103.5	
01:50:59:13	65.1	101.4	
01:50:59:14	67.5	99.2	
01:50:59:15	70.0	97.0	
01:50:59:16	72.4	94.9	
01:50:59:17	74.8	92.8	
01:50:59:18	77.1	90.8	
01:50:59:19	79.4	88.8	
01:50:59:20	81.7	86.7	
01:50:59:21	84.0	84.8	
01:50:59:22	86.2	82.8	Point C
01:50:59:23	88.5	80.8	
01:50:59:24	90.7	78.8	Point D

Point A: indicates the point where the meteor became visible in the Geigersau video. It lies inside the integration time of this frame of 40 ms.
Point B: Meteor entry in Horní Vltavice photo
Point C: Terminal flash; distance of entry point of 87.6 km, height 81.6 km
Point D: Expiration of meteor head; distance from entry point 92.9 km, height 76.9 km

4.3 Green train

In general, a green train is caused by emission in the [O I] line at 557.7 nm. The exact maxima of the colour primaries of the Sony α7S are unknown to the authors, but it is obvious that the maximum wavelength of the green channel lies below [O I] line. Hence, the green train also affects the red channel, so the resulting colour is a slightly yellowish green.

According to Figure 1 the green train becomes visible at frame 01:50:59:07 at an altitude of 114.8 km. The green train occurs "in retrospect": the end of the green train becomes brighter in the following frames. It remains visible until frame 01:51:00:15 (= 1320 ms). The brightness of the green train has two maxima: the first around frame 01:50:59:16 and the second with the terminal flash at frame 01:50:59:22. The position of the first maximum is at the position of the meteor head in frame 01:50:59:09. The brightest parts of the first maximum of green train remain visible until frame 01:51:51:12, so this part of the green train has an overall duration of 55 frames (= 2200 ms). The position of the second maximum is at the center of the terminal flash with a strong but rapidly declining afterglow from frame 01:50:59:22 until frame 01:51:01:00 (= 1120 ms). Interestingly, the longest duration of the afterglow of the green train is not at the position of the second maximum, the terminal flash, but at the position of the meteor head at frame 01:50:59:19, three frames (= 120 ms) before the terminal flash, at an altitude of 88.8 km. Here the green train remains visible nearly as long as in

Table 2 – Trajectory parameters of 3414-2018 calculated by Juergen Michelberger, Lauffen am Neckar, Germany.

Observation site 1	Geigersau (D): Peter C. Slansky/Bernd Gaehrken		
Latitude	47.728° N		
Longitude	11.027° E		
Altitude above sea level	933 m		
Azimuth to observation site 2	55.066°		
Trajectory points	Point A	Point C	Point D
Right ascension	76.180°	197.239°	199.957°
Declination	82.608°	78.535°	77.075°
Azimuth	10.969°	355.844°	354.686°
Vertical angle	49.011°	36.679°	35.421°
Distance directly	206.9 km	133.5 km	129.6 km
Distance projected on ground	132.5 km	105.7 km	104.4 km
Observation site 2	Horní Vltavice (CZ): Juergen Michelberger/Reinhardt Wurzel		
Latitude	48.952° N		
Longitude	13.765° E		
Altitude above sea level	822 m		
Azimuth to observation site 1	237.112°		
Trajectory points	Point A	Point C	Point D
Right ascension	303.232°	291.579°	290.933
Declination	28.995°	10.308°	9.139
Azimuth	268.934°	262.715°	262.403
Vertical angle	40.918°	19.942°	18.644
Distance directly	237.1 km	226.4 km	226.9 km
Distance projected on ground	174.8 km	210.2 km	212.4 km
Base line parallax	243.7 km		
Trajectory points	Point A	Point C	Point D
Parallaxes to trajectory	66.169°	80.760°	81.313°
Trajectory points	Point A	Point C	Point D
Latitude projected to ground	48.898°	48.677°	48.663°
Longitude projected to ground	11.372°	10.922°	10.895°
Altitude above sea level	158.6 km	81.6 km	76.9 km
Trajectory points	Point A to D	Point A to C	Point C to D
Distance over ground	43.55 km	41.05 km	2.51 km
Distance along trajectory	92.9 km	87.62 km	5.28 km
Meteor duration	1.575 s	1.485 s	0.090 s
Virtual trajectory angle from observation site 1	18.091°	16.523°	1.568°
Virtual trajectory angle from observation site 2	22.967°	21.636°	1.331°
Meteor entry angle at point D	61.23°		

the first maximum. In the end the green colour blends more and more into the white of the persistent train.

The afterglow of the green train shows a relatively sharp outline with a radius of about 4 km from point C as shown in Figure 8.

4.4 Terminal flash

As was explained above, at frame 01:50:59:16 the meteor head begins to bloom. This corresponds to an altitude of 94.9 km. 6 frames later, at an altitude of 82.8 km, the meteor disintegrates in a terminal flash. During these 6 frames the brightness of the meteor increases over-exponentially.

Figure 2 shows that the terminal flash causes an overexposed and clipped meteor center in the image. The clipped area is nearly perfectly round shaped with a diameter of 188 pixels, the terminal flash does not show any motion blur. Hence, the authors assume a very sharp brightness peak of the terminal flash of less than 1/10 of a frame or less than 4 ms.

Note, that the green train extends into the overexposed center. Because a white overexposed area of an image cannot be "dimmed" by additional green light, this shows that the terminal flash is not entirely round shaped but has a dimmer part at the rear, connected to the green train. This might have the same reason as the axe-shape of the halo of the 2001 Leonid observed by Jenniskens & Stenbaek-Nielsen with 1000 fps (Jenniskens & Stenbaek-Nielsen, 2004). But due to the stronger motion blur in our case, caused by the integration time of 1/25 s, this cannot be judged precisely.

In order to investigate the nature of the clipped area the authors made a series of tests with the same camera and lens. Their volume would burst the volume of this article; the methods and the results are documented in (Slansky & Gaehrken, 2018). As a result, it was impossible to reproduce a clipped area of this size by the overexposure of a point light source alone without producing other significant artefacts like lens flares. These artefacts are missing in the images. So, only an areal light source produces a high light reproduction like the one in the video.

Figure 8 (left) shows the spatial dimensions of the terminal flash: The two yellow circles indicate a radius of 2 km (inner circle) respectively 4 km (outer circle) around point C. Each white line indicates a real distance

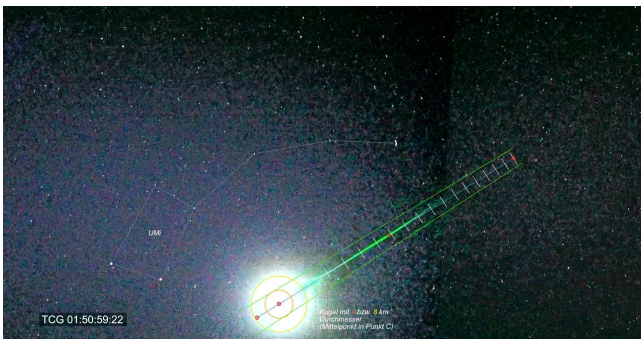

Figure 8 – Terminal flash (left). Two frames after the terminal flash (right). The two yellow circles indicate a diameter of 4 km (inner circle) and 8 km (outer circle) at point C of the trajectory. Each white line indicates a real distance along the trajectory of 5 km starting from point A (red dot on the right).

along the trajectory of 5 km starting from point A (red dot on the right). The yellow circle with the radius of 4 km fits quite well with the terminal flash. Even in the green afterglow fits to the light distribution of 3414-2018.

4.5 Afterglow of the terminal flash

The afterglow of the terminal flash is presented in Figures 9–11.

4.6 Widespread bluish sky glow

It came as a big surprise to the authors that the terminal flash was not just reflected by the sky but that a widespread bluish sky glow around the terminal flash showed a decay over up to 12 frames (= 480 ms). In the images of both cameras the bluish sky glow occurred in a very wide area around the terminal flash. To exclude camera or lens artefacts as a reason for this light effect the authors made another line of empirical tests with the same camera-lens combination. As a result, camera or lens artefacts could be excluded as a reason. The methods and results of the tests are documented in (Slansky & Gaehrken, 2018).

4.6.1 Photometry of the sky glow

To examine the brightness distribution of the meteor three separate measurements were made from each video frame: one for the meteor core in white and in green, including the meteor head, the wake, the terminal flash and its afterglow, a second one for the meteor core in green, including the green train and the green afterglow, and a third for the bluish sky glow in the red, green and blue channel. According to the huge brightness differences these measurements had to be based on different methods.

The sky glow was very dim. For its determination the opto-electronical conversion function (OECF) of the Sony α7S the original settings of the observation was measured by Peter C. Slansky with a Kodak test chart with 20 grey scales of 1/3 F-stop (Slansky, 2018b). The OECF was put into an Excel-table with the code values of the three channels RGB on the y-axis (8 Bit = 0 to 255 for red, green and blue) and the brightness in arbitrary F-stops on the x-axis. It was normalized to the sky background that was measured in the video frames before the increase of the meteor head's brightness and the terminal flash. This measurement has an error of

Figure 9 – One frame after the terminal flash. The meteor head is proceeding further from the position of the terminal flash. Note the strong green afterglow behind and around the meteor head. Its diameter is almost the same as the one of the terminal flash. Also, note the widespread bluish sky glow.

Figure 10 – Two frames after the terminal flash. The meteor head is proceeding to its terminal position where it fades away. Note the white afterglow of the wake and the strong green afterglow. Independently, the sky glow declines but remains bluish.

Figure 11 – Three frames after the terminal flash. The meteor head has faded away. Note the white afterglow of the wake and the strong green afterglow.

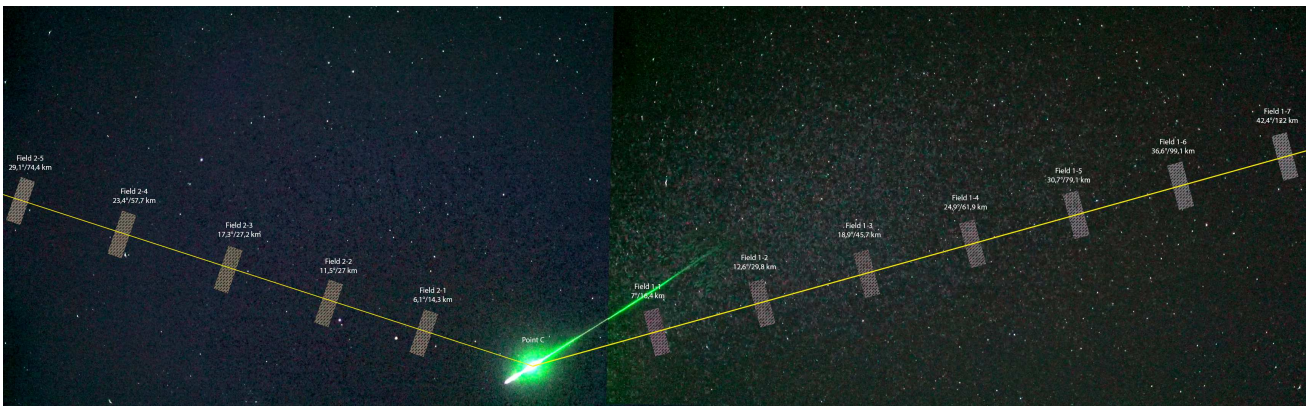

Figure 12 – Arrangement of the measurement fields for the sky glow for both cameras. In order to reduce the influence of the apparent image noise each field is 40 × 160 pixels wide, with the code values averaged. The distance from point C is indicated as an angle as well as a distance along the respective yellow line rectangular to the line from the camera to point C. A positive sign indicates the direction with the trajectory (to the left), a negative sign against the trajectory (to the right).

less than 1/10 of an F-stop or less than 7% at code values higher than 4.

The measurement of the sky glow was done separately for both cameras in an alignment of measurement fields of 40 × 160 pixels. Inside these fields the code values were averaged to eliminate the influence of the image noise. The distances of the centers of the fields from point C are indicated as an angle as well as a distance along the respective yellow line rectangular to the line from the camera to point C. A positive sign indicates the direction with the trajectory (to the left), a negative sign against the trajectory (to the right).

Left from point C five measurement fields were aligned (Table 3).

Table 3 – Measurement fields from camera 2.

Field	Angle from point C	Distance from point C	Camera
2-1	5.6°	13 km	2
2-2	12°	29 km	2
2-3	18°	43 km	2
2-4	23°	57 km	2
2-5	30°	76 km	2

Right from point C seven measurement fields were aligned. Because field 1 of camera 1 suffered strongly from sensor amplifier glowing it was superseded by field 2- -1 of camera 2 (Table 4).

Table 4 – Measurement fields from cameras 1 and 2.

Field	Angle from point C	Distance from point C	Camera
2- −1	−7.0°	−16 km	2
1-2	−13°	−30 km	1
1-3	−19°	−46 km	1
1-4	−25°	−62 km	1
1-5	−31°	−79 km	1
1-6	−37°	−99 km	1
1-7	−42°	−122.1 km	1

4.6.2 Photometry of the meteor core

Due to the strong overexposure with huge numbers of clipped pixels the brightness of the meteor core – the green train, the wake, the terminal flash and the green afterglow – had to be measured by another method. Their brightness should be compared to the bluish sky glow only relatively. Because the numbers of clipped pixels are proportional to the overexposed areas this numbers were taken as an indicator. For a comparative diagram this number was also calculated to F-stops. An absolute calibration was not necessary because the comparison was made relatively. Because of the significant differences in the distribution between the white light – the wake, the terminal flash and their afterglow – and the green light – the green train and its afterglow – separate counting of clipped pixels was made for white and green. For the white overexposed area all pixels with RGB code values 255/255/255 were counted and for the green overexposed area all pixels with RGB code values X/255/X were counted with X ≠ 255 ("green only"). The exactness of measurement of this method has not been calculated.

In this article all photometric measurements rely on images recorded by cameras. So, their results are expressed in F-stops, not in magnitudes, because magnitudes go back to the nonlinearity of the human eye: One magnitude represents a physical brightness increase (or decrease) by a factor 2.5, to be taken as a perceptual brightness increase (or decrease) by the human eye by a factor 2. Both expressions can be converted to each other easily: One F-stop equals 3/4 magnitude, one magnitude equals 4/3 F-stops.

4.6.3 Temporal brightness distribution of the sky glow

As can be seen from Figures 19 and 20, the temporal progress of brightness of the sky glow is related to the brightness progress of the meteor core but not in a linear way. Neither does the brightness of sky glow follow the brightness of the white terminal flash and the white afterglow nor the brightness of the green train and green afterglow. Also, the sky glow keeps its bluish colour nearly constantly.

In Figure 19 (bottom curves) the high value of the red channel of field 2-5 has to be ignored because it goes back to sensor amplifier glowing of the camera.

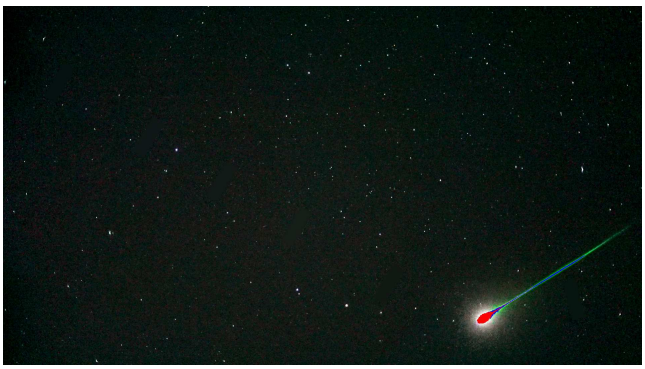

Figure 13 – Video frame 01:50:59:20 of camera 2, two frames before the terminal flash. The white overexposed pixels are indicated in red, the green overexposed pixels (green only) in blue. Counting reveals 1144 overexposed pixels white = 8.2 arbitrary F-stops and 1067 overexposed pixels green (only) = 8.1 arbitrary F-stops. The white amount and the green only amount are almost equal.

Figure 14 – Frame 01:50:59:21 of camera 2, one frame before the terminal flash: 3554 overexposed pixels white = 9.8 arbitrary F-stops and 2636 overexposed pixels green = 9.4 arbitrary F-stops. The white amount begins to dominate the green one.

Figure 15 – Frame 01:50:59:22 of camera 2, terminal flash: 11076 overexposed pixels white = 11.4 arbitrary F stops and 6077 overexposed pixels green = 10.6 arbitrary F-stops. The terminal flash is much stronger in white than in green. This cannot be caused by a strong green overexposure, because than a green halo would be seen. But the halo around the terminal flash is white. Additionally, a bluish sky glow appears. (Also, the averaging of the code values inside the measurement fields can be seen.) The rectangular structures around and behind the meteor head are data compression artefacts caused by the camera.

Figure 16 – Video frame 01:50:59:23 of camera 2, one frame after the terminal flash: 3172 overexposed pixels white = 9.6 arbitrary F-stops and 5255 overexposed pixels green = 10.4 arbitrary F-stops. It is quite remarkable that even in the first frame after the terminal flash the green begins to dominate the white due to its much longer persistence.

Figure 17 – Video frame 01:50:59:24 of camera 2, two frames after the terminal flash: 978 overexposed pixels white = 7.9 arbitrary F-stops and 5433 overexposed pixels green = 10.4 arbitrary F-stops. Only two frames after the terminal flash the dominance of the green over the white has become drastic.

Figure 18 – Video frame 01:51:00:00 of camera 2, three frames after the terminal flash: 495 overexposed pixels white = 7.0 arbitrary F-stops and 4770 overexposed pixels green = 10.2 arbitrary F-stops. As can be seen from this sequence, the white light and the green light have different temporal distributions: The white has a higher maximum but a more sudden decline compared to the green with a lower maximum but a longer persistence. The widespread sky glow does not follow the change in colour of the meteor core from white to green only.

Figure 20 shows the brightness of the sky glow in the direction against the trajectory.

Please note that in Figure 20 field 2- -1 of camera 2 was used instead of field 1 of camera 1, because the former suffered strongly from sensor amplifier glowing.

As can be seen from Figures 15–18 and graphs in Figures 19 and 20, until the terminal flash the brightness of the white parts of the meteor core (black circles in Figure 19) dominate the green parts (dark green triangles in Figure 19). In the first frame after the ter-

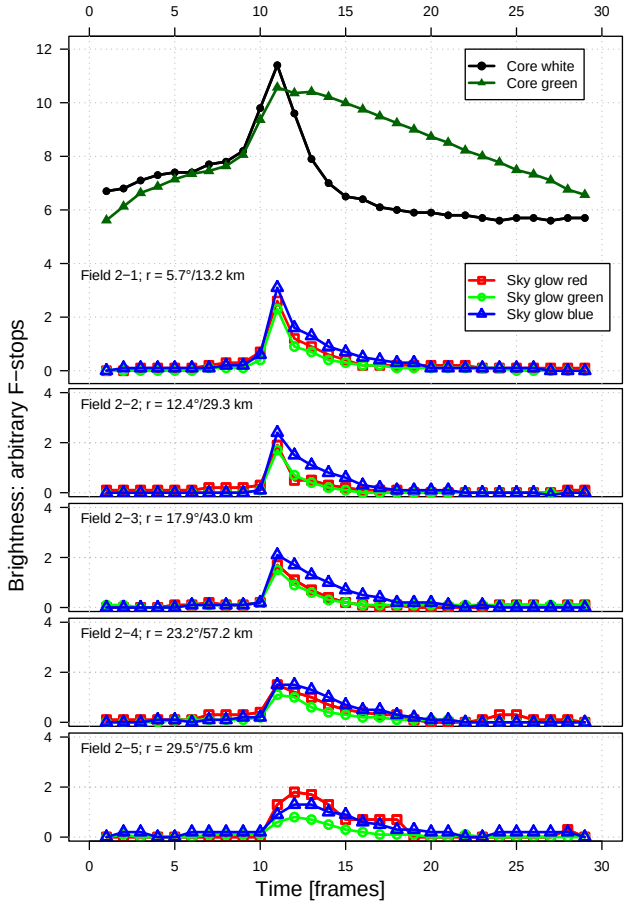

Figure 19 – The brightness of the sky glow in the direction with the trajectory.

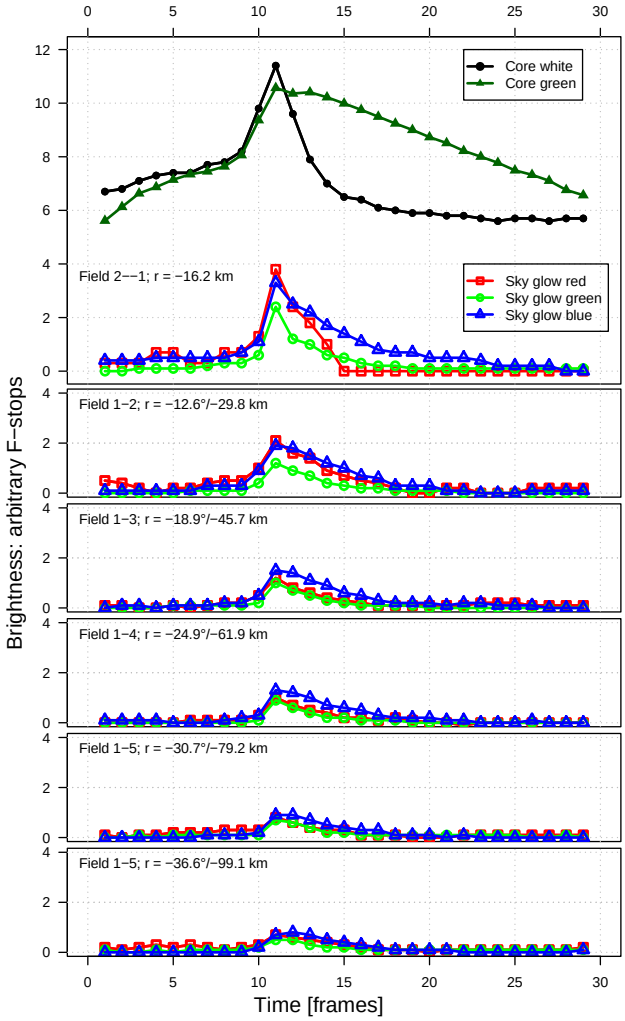

Figure 20 – The brightness of the sky glow in the direction against the trajectory.

minal flash the green parts begin to dominate, showing a much longer persistence than the white parts of the core. But the sky glow does not follow this drastic transient. It keeps its bluish colour throughout. Also, its persistence lasts longer than that of the white parts of the core (see black curve in Figure 19).

To the knowledge of the authors, such a phenomenon has not been reported before.

Because of this temporal brightness and colour development, the sky glow cannot be caused be reflection of the meteor in the earth's atmosphere alone. Diffuse reflection can only do a small contribution to this sky glow. Mainly, it must have other physical reasons.

Another remarkable detection is the spatial dimensions of the sky glow. As expressed in Figures 19 and 20, it is visible with a similar temporal development in both cameras and in all 12 measurement fields. The most remote field of camera 1 is field 1-7 with an angular distance from point C of 42.4° or 122 km, of camera 2 it is field 2-5 with an angular distance from point C of 29.5° or 75.6 km.

A last striking issue is a dark void inside the widespread sky glow with its center about 8.5° or 20 km of from point C on the upper left side. According to Figure 19 (fields 2-2, 2-3, and 2-4), beginning in the frame after the terminal flash – frame 12 in the respective tables – until frame 17 the sky glow is remarkably darker in fields 2-1 and 2-2 than in the more remote fields 2-3 and 2-4. This dark void remains stationary for about five frames = 200 ms. It cannot be explained by camera or lens artefacts.

4.7 Persistent train

The persistent train of 3414-2018 started at a height of 100 km and ended at a height of 79 km with a length of 30 km. He was recorded with two cameras, the Sony α7s in video mode 25 fps and a Canon EOS M that provided a photo series. The EOS M is an APS-C format camera. It was equipped with a 2.8/50mm lens. The exposure time was 15 seconds at ISO 3200.

On the Sony video, the persistent train is completely visible and its development is easy to follow (Slansky, 2018c). The end of the wake and the beginning of the persistent train are difficult to separate. The brightness measurement of the persistent train starts two seconds after the end of the terminal flash. At this time, only small parts of the track burned out and the remains of the wakes have disappeared.

The EOS M exposure time of 15 s was 375 times longer than the exposure time of the Sony α7s of 1/25 s. On the other side, the sensitivity of the EOS M of ISO 3200 and that of the Sony ISO 409 000 and the lens of the EOS M had an aperture of 2.8 while the lens of the Sony had an aperture of 1.4. But the longer

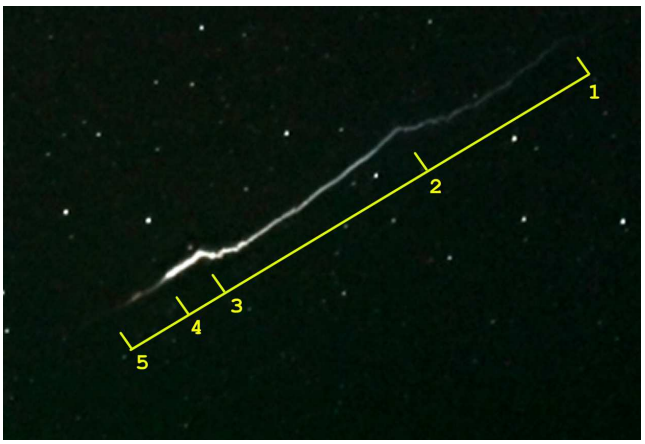

Figure 21 – The persistent train in an overlay of 25 video frames at time code 01:51:06.

Table 5 – Height of points 1–5 in Figure 21.

Point in Figure 21	1	2	3	4	5
Height [km]	100	92	82	81	79

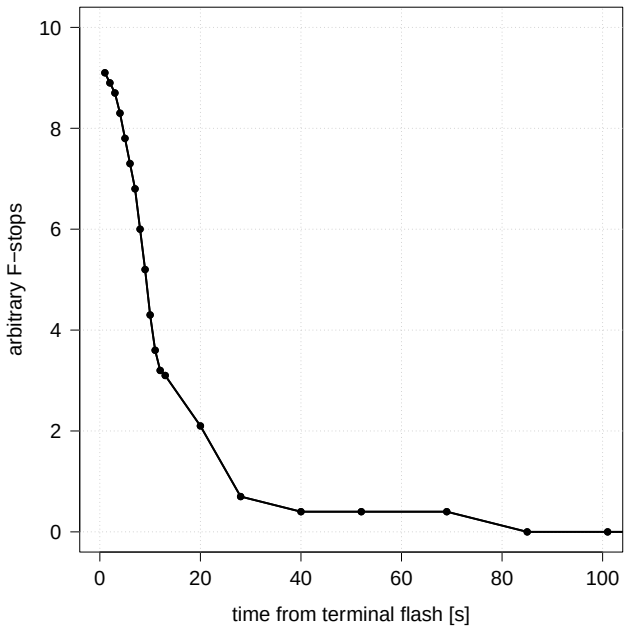

Figure 22 – Brightness development of the persistent train measured over 2.5 minutes.

exposure time of the EOS M and the lower ISO setting provided a better signal-to-noise-ratio and higher colour saturation. So, in the photo series of the EOS M shown in Figure 3 the persistent train could be detected better, over a duration time of 7 minutes before the photo series was stopped. The colour gradient from blue to red that is typical for a fresh persistent train is still clearly visible on the first picture after the fall. On the second picture after the fall, the blue has faded and all other pictures show a uniform brown-yellowish colour.

In Figure 21 five points are marked. Table 5 shows their respective height.

At 01:51:06 UT, six seconds after the terminal flash, the persistent train is showing signs of disintegration, as it breaks up into several sections. The reason for the kinks at points 2 and 3 in Figure 22 are different vertical winds in the high atmosphere.

The first and the last section of the train faded very fast. At points 2, 3 and 4 an attempt to measure the development of the brightness was made. However, it lacked a three-dimensional model that enabled a calculation of the changing column density with the perspective of the photo series. Therefore, at least the brightness development of the total curve was determined. This measurement was corrected with the OECF of the video camera (see Section 4.6.1). The result is shown in Figure 22. It shows three sectors: In the first 12 seconds there is a strong decrease in brightness by a factor 63 = 6 F-stops. After that, the curve flattens considerably: Between the twelfth and the twenty-eighth second the brightness drop is only factor 5.6 = 2.5 F-stops. From the twenty-eighth second on the brightness drop is very flat. The persistent train is still visible but cannot be measured properly for the next 100 seconds.

4.8 Radio Observation

Wolfgang Kinzel sent the authors a radio diagram of a long meteor trail echo. By the exact time and the long trail echo there could be no mistake: That was 3414-2018. He had observed the fireball from Dessau, Saxony-Anhalt, 51°48'06.46" N / 12°15'22.01" E, 65 m altitude, with a four-element yagi antenna in the 2-meter band at 143.050 MHz, pointed to the GRAVES radar in France, with an azimuth of 221° SW, elevation 20°, 3 m over ground level. The distance Dessau-GRAVES is 694 km. Because the main direction of the GRAVES radar is south, the trail echo must come from one of the northern secondary lobes of the radar.

The interpretation of the radiogram was given by Wolfgang Kaufmann, Algermissen. Figure 23 shows two typical meteor head echoes, A and C. B is a meteor trail echo of about 100 ms. This duration meets the majority of radio meteors. According to the exact timing, D is the trail echo of 3414-2018. It lasts 43 s and has a Doppler shift of 35 Hz at the maximum. The Doppler shift is estimated to be caused mainly by wind drift that affects different parts of the trail in different heights in different ways and directions. This is estimated to a tree-dimensional warping of the trail that can be seen in the photo series of the persistent train (Figure 3), too. Additionally, the radio waves reflected by the different trail segments reach the receiver with different phasing. This explains the oscillation of the signal amplitude. At the end the trail echo occurs more and more interrupted. This might also go back to wind drift changing the geometry of radio wave reflection. The radiogram does not show indications for fragmentation.

Parallel observations of meteorites in the visual and the radio range are still rare and a comparison with the visual ZHRs is difficult. But with only one video observation and one radio observation from different positions three-dimensional calculations cannot be made. In order to better understand the context, especially in the interpretation of the Doppler shift, it would make sense to expand parallel observations, as well in video as in radio.

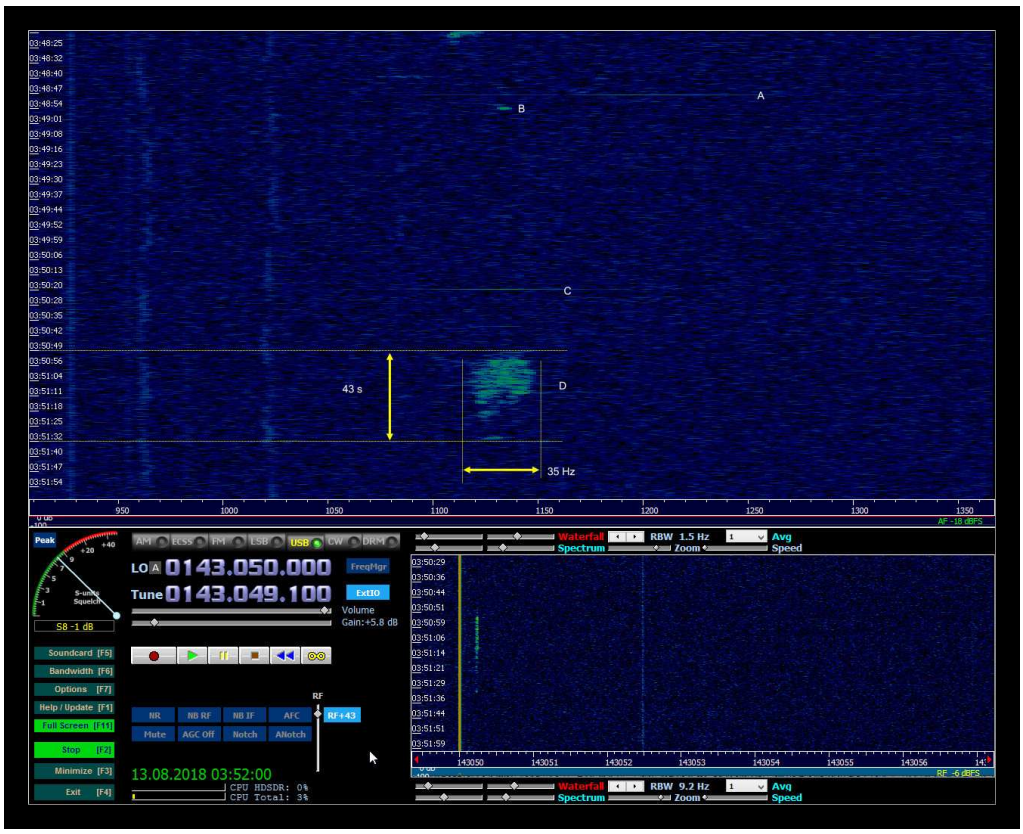

Figure 23 – Radiogram of 3414-2018 by Wolfgang Kinzel, Dessau, Saxony-Anhalt, 51°48'06.46" N / 12°15'22.01" E, 65 m altitude. The observation was made with a four-element yagi antenna in the 2-meter band at 143.050 MHz, pointed to the GRAVES radar in France, with an azimuth of 221° SW and elevation 20°, 3 m over ground level.

5 Discussion

The light distribution of 3414-2018 shows several remarkable peculiarities. The observations were possible only by the use of two very high sensitive cameras in video mode with full HD resolution in colour.

Referring to Figure 2 the terminal flash shows a nearly perfect circular shape, but with a significant green strangling on the rear which is connected directly to the green train. This might have similar reasons as the axe-shape of the halo of the 2001 Leonid, observed by Jenniskens & Stenbaek-Nielsen (2004). Due to the stronger motion blur caused by an integration time of 1/25 s this cannot be judged precisely (Jenniskens & Stenbaek-Nielsen, 2004).

The spatial dimensions of the terminal flash and the green afterglow of 3414-2018 with a radius up to 4 km are exceptional. This goes back to advances in the observing technique compared to observations with older analog monochrome CCD cameras with SD resolution that are still widely in use in meteor observation.

For the 2001 Leonid observed by Jenniskens & Stenbaek-Nielsen, Šiljić et al. (2018) report a brightness gradient of 1 km from the meteor heads center the brightness fallen down to 1/30 of the maximum at an altitude of 104.8 km. (The measurement was not executed to wider distances.) It has to be taken into account that the exposure of the images has a huge influence on measurements like this. It would be very valuable to detect brightness gradients of meteors via high dynamic range imaging.

There is also reasonable conformity between fireballs 3414-2018 and EN120812 observed by Spurný et al. (2014): Both show terminal flashes with a very sharp brightness increase on nearly the same altitude (Table 6).

According to Wurzel & Michelberger (2005) the air density is increasing significantly at this altitude.

Spurný et al. (2014) divided the appearance of high altitude meteors into three distinct phases: diffuse, intermediate and sharp. The diffuse phase was observed and described by Gaehrken/Michelberger for a high altitude Leonid 2002 (Gaehrken & Michelberger, 2003). According to this, the similarities between 3414-2018 and EN120812 indicate similar physical formation conditions.

The diffuse, widespread bluish sky glow of 3414-2014 has been recorded by two cameras independently: Camera 2 with the terminal flash in its field of view as well as camera 1 with the terminal flash outside its field of view. The bluish sky glow can be seen up to an angle of 42° – respectively a distance of 122 km – from the point of the terminal flash. Its bluish colour does not follow the drastic change in colour from the white terminal flash to the green afterglow with a much longer persistence. Hence, diffuse reflection contributes only a minor part to the sky glow, but cannot be its major physical reason. Also, the temporal development of the brightness as well as the colour of the sky glow does neither follow the development of the white part of the meteor core nor the one of the green part. Again, the

Table 6 – Brightness developments along the trajectories of Perseid fireballs 3414-2018 and EN120812.

	Altitude of entry	Altitude of terminal flash	Altitude of expiration
3414-2018	158.6 km	81.6 km	76.9 km
EN120812	170.2 km	82.7 km	78.6 km

physical reasons must be different from diffuse reflection in the earths' atmosphere alone.

There are different scientific approaches for the explanation of the physical nature of meteors' light emissions, for example electric charge and magnetic fields around the meteor (Šiljić et al., 2018), UV-radiation (Jenniskens, 2004) or X-rays (Smirnov, 2015). Because the authors are amateur meteor observers they will not exceed their competence by speculation. But they are ready to discuss and share their observations and data with every interested scientist.

Acknowledgements

The authors want to thank Juergen Michelberger and Reinhardt Wurzel for their engaged cooperation on the observation and analysis of 3414-2018, especially for the calculation of the trajectory. The authors also thank Wolfgang Kinzel for obtaining his radio observation and Wolfgang Kaufmann for its interpretation. Thank also goes to Rudolf Sanda, Austria, Christ Steyaert, Belgium, and Giancarlo Tomezzoli, Germany, for additional information about the radiogram.

References

Gaehrken B. (2018). "Perseiden 2018". http://www.astrode.de/8perseiden18a.htm

Gaehrken B. and Michelberger J. (2003). "A bright, high altitude 2002 Leonid". *WGN, Journal of the IMO*, **31:5**, 137–138.

Hughes D. W. (1995). "The Perseid meteor shower". *Earth Moon and Planets*, **68**, 31–70.

IMO (2014). "Events in 2014: 3638-2014". https://fireballs.imo.net/members/imo_view/event/2014/3638

IMO (2017). "Events in 2017: 4299-2017". https://fireballs.imo.net/members/imo_view/event/2017/4299

IMO (2018). "Events in 2018: 3414-2018". https://fireballs.imo.net/members/imo_view/event/2018/3414

Jenniskens P. (2004). "Meteor storms as a window on the delivery of extraterrestrial organic matter to the early Earth". In Norris R. P. and Stoothman F. H., editors, *Bioastronomy 2002: Life Among Stars, IAU Symposium*, volume 213. IAU, pages 281–288.

Jenniskens P. and Stenbaek-Nielsen H. C. (2004). "Meteor wake in high frame-rate images and implications for the chemistry of ablated organic compounds". *Astrobiology*, **4:1**, 95–108.

Rendtel J. (2017). "2018 Meteor Shower Calendar". IMO_INFO(2-17).

Slansky P. C. (2016). "Meteor film recording with digital film cameras with large CMOS sensors". *WGN, Journal of the IMO*, **44:6**, 190–197.

Slansky P. C. (2018a). "The efficiency of cameras for video meteor observation and a theoretical contribution and a practical comparison between the Watec 120N+ and the Sony α7S". *WGN, Journal of the IMO*, **46:1**, 24–29.

Slansky P. C. (2018b). "Opto-electronical conversion function of the Sony α7S with standard gamma". http://slansky.userweb.mwn.de/bereiche/astronomie/aufnahmetechniken/bilder/oecf_sony-a7s.pdf .

Slansky P. C. (2018c). "Time lapse sequence of 3414-2018". http://slansky.userweb.mwn.de/bereiche/astronomie/meteore/perseiden-bolid_13-08-2018_03-51_03a.html

Slansky P. C. (2019). "SCAMPI - Single Camera Measurement of the Population Index". In ??, editor, *Proceedings of the International Meteor Conference, Pezinok, Slovakia, 2018.* International Meteor Organization, page ??

Slansky P. C. and Gaehrken B. (2018). "Camera test of the Sony α7S with a Canon FD 1.4/50 mm lens about blooming of overexposed highlights in regard of the video observation of fireball 3414-2018". http://slansky.userweb.mwn.de/bereiche/astronomie/aufnahmetechniken/bilder/camera-test_sony-a7s_3414_2018.pdf

Smirnov V. A. (2015). "About the nature of meteor flares". *Odessa Astronomical Publications*, **28**, 58.

Spurný P., Shrbený L., Borovička J., Koten P., Vojáček V., and Štork R. (2014). "Bright Perseid fireball with exceptional beginning height of 170 km observed by different techniques". *Astronomy & Astrophysics*, **563**, A64.

Šiljić A., Lunić F., Teklić J., and Vinković D. (2018). "Proton-induced halo formation in charged meteors". *MNRAS*, **481**, 2858–2870.

Wurzel R. (2019). "Eine Feuerkugel der Extraklasse". *Sterne und Weltraum*, **58:8**, 62–69.

Wurzel R. and Michelberger J. (2005). "Earthgrazer – Wunder des Himmels". *Sterne und Weltraum*, **44:11**, 76–83.

Handling Editors: Željko Andreić and Javor Kac

The International Meteor Organization

www.imo.net

Follow us on Facebook InternationalMeteorOrganization

Follow us on Twitter @IMOMeteors

Council

President: Cis Verbeeck,
Bogaertsheide 5, 2560 Kessel, Belgium.
e-mail: cis.verbeeck@scarlet.be

Vice-President: Juraj Tóth,
Fac. Math., Phys. & Inf., Comenius Univ.,
Mlynska dolina, 84248 Bratislava, Slovakia.
e-mail: toth@fmph.uniba.sk

Secretary-General: Robert Lunsford,
14884 Quail Valley Way, El Cajon,
CA 92021-2227, USA. tel. +1 619 755 7791
e-mail: lunro.imo.usa@cox.net

Treasurer: Marc Gyssens, Heerbaan 74,
B-2530 Boechout, Belgium.
e-mail: marc.gyssens@uhasselt.be
BIC: GEBABEBB
IBAN: BE30 0014 7327 5911
Bank transfer costs are always at your expense.

Other Council members:

Megan Argo, Jodrell Bank Centre for Astrophysics,
Alan Turing building, University of Manchester,
Oxford Road, Manchester, M13 9PL, UK.
e-mail: megan.argo@gmail.com

Javor Kac (see details under WGN)

Detlef Koschny, Zeestraat 46,
NL-2211 XH Noordwijkerhout, Netherlands.
e-mail: detlef.koschny@esa.int

Masahiro Koseki, 4-3-5 Annaka, Annaka-shi,
Gunma-ken 379-0116, Japan.
e-mail: geh04301@nifty.ne.jp

Sirko Molau, Abenstalstraße 13b, D-84072 Seysdorf,
Germany. e-mail: sirko@molau.de

Jean-Louis Rault, Société Astronomique de France,
16, rue de la Vallée, 91360 Epinay sur Orge,
France. e-mail: f6agr@orange.fr

Jürgen Rendtel, Eschenweg 16, D-14476 Marquardt,
Germany. e-mail: jrendtel@aip.de

Paul Roggemans, Pijnboomstraat 25, 2800 Mechelen,
Belgium, e-mail: paul.roggemans@gmail.com

Galina Ryabova, Res. Inst. of Appl. Math. & Mech.,
Tomsk State University, Lenin pr. 36, build. 27,
634050 Tomsk, Russian Federation.
e-mail: ryabova@niipmm.tsu.ru

Damir Šegon, J. Rakovca 3, 52100 Pula, Croatia.
e-mail: damir.segon@pu.t-com.hr

Commission Directors

Visual Commission: Rainer Arlt (rarlt@aip.de)
Generic e-mail address: visual@imo.net
Electronic visual report form:
http://www.imo.net/visual/report/electronic

Video Commission: Sirko Molau (video@imo.net)

Photographic Commission: Bill Ward
(William.Ward@glasgow.ac.uk)
Generic e-mail address: photo@imo.net

Radio Commission: Jean-Louis Rault (radio@imo.net)

Fireballs: Online fireball reports:
http://fireballs.imo.net

Outreach Officer

Jure Atanackov, e-mail: jureatanackov@gmail.com

Webmaster

Karl Antier, e-mail: webmaster@imo.net

WGN

Editor-in-chief: Javor Kac
Na Ajdov hrib 24, SI-2310 Slovenska Bistrica,
Slovenia. e-mail: wgn@imo.net;
include METEOR in the e-mail subject line

Editorial board: Ž. Andreić, M. Argo, D.J. Asher,
F. Bettonvil, J. Correira, M. Gyssens,
C. Hergenrother, T. Heywood, J.-L. Rault,
J. Rendtel, C. Verbeeck, S. de Vet, D. Vida.

IMO Sales

Available from the Treasurer or the Electronic Shop on the IMO Website	€	$
IMO membership, including subscription to WGN Vol. 47 (2019)		
Surface mail	26	32
Air Mail (outside Europe only)	49	60
Electronic subscription only	21	25
Proceedings of the International Meteor Conference on paper		
1990, 1991, 1993, 1995, 1996, 1999, 2000, 2002, 2003, per year	9	12
2007, 2010, 2011, per year	15	20
2012, 2013, 2014, 2015 per year	25	34
Proceedings of the Meteor Orbit Determination Workshop 2006	15	20
Radio Meteor School Proceedings 2005	15	20
Handbook for Meteor Observers	15	20
Meteor Shower Workbook	12	16
Electronic media		
Meteor Beliefs Project ZIP archive	6	8